ELSEVIER

NeuroImage

www.elsevier.com/locate/ynimg
NeuroImage 36 (2007) 736–745

A validated network of effective amygdala connectivity

Jason L. Stein,[a,b,c] Lisa M. Wiedholz,[b,c] Danielle S. Bassett,[a] Daniel R. Weinberger,[c] Caroline F. Zink,[a,c] Venkata S. Mattay,[b,c] and Andreas Meyer-Lindenberg[a,b,c,*]

[a]*Unit for Systems Neuroscience in Psychiatry, Bethesda, MD 20892-1257, USA*
[b]*Neuroimaging Core Facility, Bethesda, MD 20892-1257, USA*
[c]*Clinical Brain Disorders Branch, Genes, Cognition and Psychosis Program, National Institute of Mental Health, NIH, DHHS, 10-3C103, 9000 Rockville Pike, Bethesda, MD 20892-1257, USA*

Received 20 December 2006; revised 28 February 2007; accepted 17 March 2007
Available online 28 March 2007

Regulatory interactions with the amygdala are thought to be critical for emotional processing in the extended limbic system. Structural equation modeling (path analysis) is a widely used method to quantify interactions among brain regions based on connectivity models, but is often limited by lack of precise anatomical and functional constraints. To address this issue, we developed an automated elaborative path analysis procedure guided by known anatomical connectivity in the macaque. We applied this technique to a large human fMRI data set acquired during perceptual processing of angry or fearful facial stimuli. The derived models were inferentially validated using a bootstrapping split-half approach in pairs of 500 independent groups. Significant paths across the groups were used to form a rigorously validated and consistent path model. We confirm and extend previous observations of amygdala regulation by an extended prefrontal network encompassing cingulate, orbitofrontal, insular, and dorsolateral prefrontal cortex, as well as strong interactions between amygdala and parahippocampal gyrus. This validated model can be used to study neurocognitive correlates as well as genotype or disease-related alterations of functional interactions in the limbic system.
Published by Elsevier Inc.

Introduction

The limbic system is essential to emotional processing (LeDoux, 2000). The amygdala is a critical node in this network, and is necessary for imbuing percepts with affective significance, especially for fearful or dangerous environmental stimuli (Amaral and Price, 1984; LeDoux, 2000). In agreement with this, studies of patients with lesions in the amygdala (Adolphs et al., 1994) have consistently shown deficits in the ability to identify the affect of faces. Functional neuroimaging studies have also implicated amygdala activity in fear response (Morris et al., 1996; Hariri et al., 2000) with highest amygdala response to fearful or angry faces.

However, while the amygdala is a central part of the neural circuitry for emotion, it does not operate in isolation. In fact, the importance of functional interconnectedness between component structures of the "limbic lobe" was stressed even in 1937, when Papez emphasized their "harmonious mechanism" as the basis of emotional regulation (Papez, 1995). Functional interactions between component structures in the limbic system are wide-ranging. Tracer studies in macaque monkeys show that the amygdala is extensively anatomically connected with cortical areas including cingulate, prefrontal cortex, parahippocampal gyrus, and insula (Barbas and De Olmos, 1990; Amaral and Price, 1984; Ghashghaei and Barbas, 2002; Stefanacci et al., 1996) and subcortical areas including the hippocampus (Saunders et al., 1988). Therefore, defining the functional limbic network is expected to provide a better characterization and classification of healthy and abnormal function related to emotional cognition and regulation. Network definition requires neuroimaging methodology which takes functional interconnections into specific account. Here, we use structural equation modeling (SEM) or path analysis, a procedure to identify directional interaction among regions given the pairwise correlations of their time series, in a large data set of 83 healthy humans scanned during a well-validated task involving perceptual judgment on angry and fearful faces (Hariri et al., 2002).

SEM has been applied in functional neuroimaging for over a decade (McIntosh and Gonzalez-Lima, 1994; Bullmore et al., 2000; Steele et al., 2004). Despite its wide acceptance in the field, applying SEM to neuroimaging data is not straightforward. One important difficulty comes from the fact that results from SEM as it is commonly used are only inferential insofar as they support or do not support an *a priori* model of connectivity. This poses a problem since our current anatomical knowledge often does not constrain modeling of interactions to a sufficient degree in the highly interconnected limbic system.

To overcome this obstacle, we used an elaborative approach: we started with a "nuclear model" specifying only a small number of very well validated connections (Ghashghaei and Barbas, 2002;

* Corresponding author. 10-3C103, 9000 Rockville Pike, Bethesda, MD 20892-1257, USA. Fax: +1 301 480 0169.
E-mail address: andreasm@mail.nih.gov (A. Meyer-Lindenberg).
Available online on ScienceDirect (www.sciencedirect.com).

1053-8119/$ - see front matter. Published by Elsevier Inc.
doi:10.1016/j.neuroimage.2007.03.022

Paus, 2001; Phillips et al., 2003) and then used a data-driven search algorithm (Bullmore et al., 2000; Sorbom, 1989) to iteratively add paths, constrained by known anatomical connectivity (Kötter, 2004), until a parsimonious model was formed. Since the final model selected was thus guided by the data, it is possible that derived paths might reflect noise in the sample and not the inherent causal structure of the data. To guard against this eventuality of over-fitting and to provide a stringent test of the derived model, a bootstrapping approach was used in which the subject pool was combined into pairs of 500 independent groups, with each group containing 20 subjects, in order to verify the models. For each pair, a path model was independently derived on the first group of the data and then forced upon the second group for inferential validation. Significant paths across the first group of each pair were used to form a rigorously validated and consistent path model.

Our results show that a well-fitting model of limbic circuitry can be derived and statistically validated from functional MRI. The properties of the model confirm and extend current knowledge about functional interactions in the human limbic system and provide a framework of effective connectivity that can be used to study genetic and disease-related variation across individuals.

Materials and methods

The automated path analysis procedure used on the first group of each pair is shown graphically in Fig. 1 and largely follows

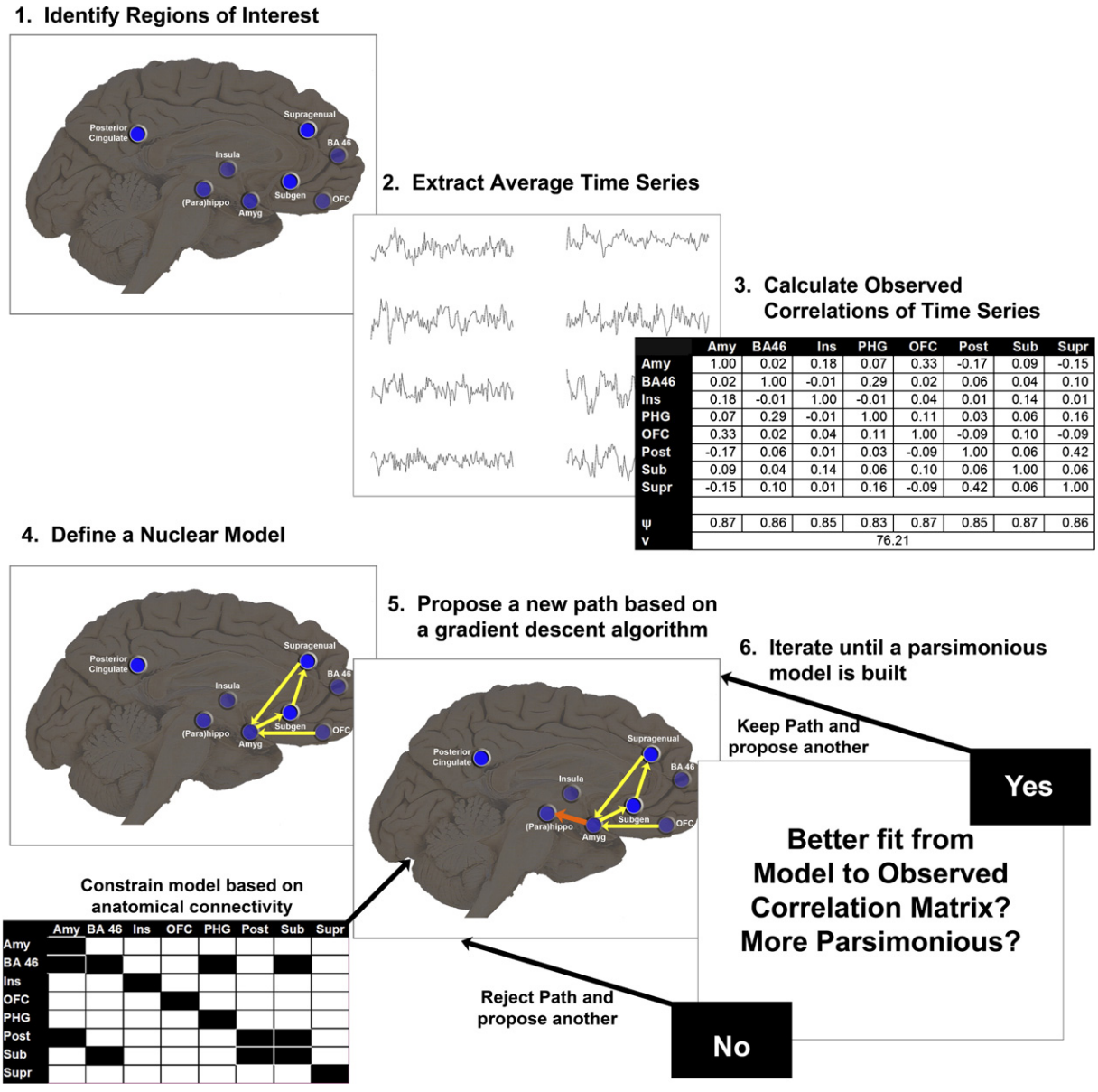

Fig. 1. Methodology for automated path analysis procedure used to generate one model. Regions of interest were selected and an inter-correlation matrix was made from the average across subjects of the time series for each region. An elaborative path analysis procedure was then used to iteratively add paths (orange arrow) to a predefined nuclear model (yellow arrows) constrained by anatomical connectivity until a parsimonious model was formed. The off diagonal terms in the anatomical connectivity matrix (lower left corner) colored black represent paths with known evidence against a direct anatomical connection that were rejected from the model.

Bullmore et al. (2000) with exceptions in the use of modification index (Sorbom, 1989), estimate of effective degrees of freedom (Kruggel et al., 2002), model build based on a nuclear model, and correlations derived from residual activity as discussed below.

Subjects

Eighty-three healthy subjects (33 male, age=28.27±7.92, Edinburgh Handedness Inventory=0.92±0.09) gave written informed consent and participated in an ongoing study according to the guidelines of the National Institute of Mental Health Institutional Review Board (Bertolino et al., 2001). Subjects were screened for and cleared of neurological, psychiatric, or substance abuse history and had no history of other significant medical problems. All available scans of subjects meeting inclusion criteria (handedness >0.8 and 18≤age≤50) and of sufficient quality (see below) were used. Data from subjects including the present cohort from this ongoing experiment have been published previously (Meyer-Lindenberg et al., 2006; Pezawas et al., 2005).

The data were randomly sampled (without replacement) 500 times to create pairs of two groups containing 20 subjects each. Within each pair, groups were matched for age, gender, and handedness, using an independent 2-sample *t*-test with a threshold of $P>0.05$ as criterion.

Experimental paradigm and image processing

During a block design face matching paradigm described previously (Hariri et al., 2002), subjects were asked to match one of two simultaneously presented faces with negative emotional affect, fear and anger (Ekman and Friesen, 1976) to an identical target image. As a control task, subjects were asked to match geometric shapes in a similar way. Four blocks of face matching served as the activation task which was interleaved with five blocks of control matching. Subjects were scanned using a GE Signa 3T scanner (Milwaukee, WI) using a gradient echo EPI sequence designed for BOLD fMRI (24 axial slices, 4 mm thickness, 1 mm gap, TR/TE=2000/28 ms, FOV=24 cm, matrix=64×64). Images were processed as described previously (Meyer-Lindenberg et al., 2006) using SPM99 (http://www.fil.ion.ucl.ac.uk/spm/).

Images were realigned to the middle image of the scan run, spatially normalized into a standard stereotactic MNI space using an affine and nonlinear transformation, smoothed with an 8-mm FWHM Gaussian filter, and ratio normalized to the whole-brain global mean. A statistical image for the contrast of emotional faces versus the control task was obtained for each subject. The functional MRI data were quality checked and clear of artifacts and low signal to noise ratio.

Region selection

Eight brain regions in the left hemisphere were selected based on prior knowledge of their interaction in an emotional network and activation or functional connectivity to the amygdala (Mayberg et al., 1999; Meyer-Lindenberg et al., 2005; Pezawas et al., 2005). The selected regions were supragenual cingulate (Brodmann Area (BA) 32), subgenual cingulate (BA 25), posterior cingulate (BA 23), orbitofrontal cortex (BA 11), parahippocampal gyrus including hippocampus (PHG), lateral prefrontal cortex (BA 46), amygdala, and insula. Eight millimeter radius spherical masks were placed at the chosen coordinates, which were guided by two lines of inquiry: (1) previously published (Meyer-Lindenberg et al., 2005; Pezawas et al., 2005) locations as well as (2) coordinates of highest activation, deactivation, or connectivity to the amygdala in a sample largely the same as the entire subject pool sample, as ascertained by a second-level random effects analysis. The selected regions and their coordinates are shown in Table 1. In order to gain functional specificity and obtain regionally specific gray matter masks, the spherical masks were then intersected with binarized functional activation maps (from the one-sample *t*-test of functional activation) thresholded at $P<0.05$ FDR corrected for multiple comparisons. In this way, all studied voxels were guaranteed to show significant task-related differential activity or functional connectivity to the amygdala through the duration of the task.

Known anatomical connectivity in the macaque monkey

It is possible that an automated path analysis procedure could derive connections that are not directly anatomically based. These connections could, for example, reflect interactions that are mediated by other regions or arise spuriously in the context of an incorrectly specified anatomical model (McIntosh and Gonzalez-Lima, 1994). To take this source of confounds into account, the model search was constrained to reject paths with known evidence against a direct anatomical connection. Since human data are incomplete, we used studies of the macaque monkey, determined largely using the Collations of Connectivity on the Macaque Brain (CoCoMac) database (www.cocomac.org) (Kötter, 2004) and supplemented by literature searches from Pubmed (http://www.ncbi.nlm.nih.gov/entrez/query.fcgi?DB=pubmed) specifying the names of the regions. Only those connections with all positive evidence against their existence according to our operational definition were excluded from the model. Table 2 includes references for each path's anatomical connectivity. Since known anatomical connectivity in the macaque does not constrain a path model enough to allow for an identified model, an automated path analysis procedure (described below) was used to iteratively add paths to build a parsimonious model.

Interregional correlation matrix

The median time series for all voxels in each of the p regional masks (here $p=8$) was extracted for each subject. Sustained shifts in BOLD relative to the presence of task were removed to

Table 1
Coordinates for regions used in modeling

Region	MNI coordinates
Supragenual cingulate (BA 32)	0 34 30
Subgenual cingulate (BA 25)	0 15 −14
Orbitofrontal cortex (BA 11)	−46 31 −9
(Para) Hippocampal gyrus	−26 −19 −14
Lateral prefrontal cortex (BA 46)	−56 26 25
Amygdala	−26 0 −20
Posterior cingulate (BA 23)	0 −33 38
Insula	−40 0 10

The MNI coordinates for each region are shown. 8 mm radius spherical masks were made around each of these coordinates and then intersected with maps of functional activation, deactivation, or connectivity to the amygdala during the task.

Table 2
Matrix of anatomical connectivity in the macaque monkey

	Amygdala	Lateral PFC (BA 46)	Insula	OFC (BA 11)	PHG	Posterior cingulate (BA 23)	Subgenual (BA 25)	Supragenual (BA 32)
Amygdala	<>	1 (SA00-46:SA00-Ld)	X (MM82a-INS:MM82c-amg)	1 (SA00-11:SA00-Ld)	Y (Stefanacci et al. (1996); Saunders et al. (1988))	X (Al92-25:Al92-Bi)	X (Al92-25:Al92-Bmg)	X (SA00-32:SA00-Ldi)
Lateral PFC (BA 46)	0 (PCG81-amg:W40-46)	<>	X (MM82a:W40-46)	X (PP99-11:PP99-46)	0 (Insausti and Munoz (2001))	X (B88-23:B88-46v)	0 (CCTCR00-25:CCTCR00-46)	X (PP99-32:PP99-46)
Insula	X (CP95a-Abpc:CP94-Lai)	Y (Mufson and Mesulam (1982))	<>	Y (Mufson and Mesulam (1982))	N	Y (Mufson and Mesulam (1982))	1 (CP94-25:CP94-Iapm)	3 (CP94-32:CP94-Iai)
OFC (BA 11)	X (PCG81-amg:W40-11)	3 (CP94-46:SA94A-11)	X (B88-Id:B88-11)	<>	Y (Morecraft et al. (1992); Cavada et al. (2000))	X (B88-23:B88-11)	X (B88-25:B88-11)	3 (CP94-32:AP84-11)
PHG	Y (Stefanacci et al. (1996))	N	N	Y (Insausti and Munoz (2001))	<>	N	N	N
Posterior Cingulate (BA 23)	0 (AP84-B:AP84-23)	1 (PP94-46:VPR87-23)	X (JB76a-Id:VPR87-23)	1 (PP94-11:MCSGP04-23)	Y (Kobayashi and Amaral (2003))	<>	0 (VPR87-25:VPR87-23)	1 (PP94-32:VPR87-23)
Subgenual (BA 25)	X (AP84-B:AP84-25)	0 (BP89-46:BP89-25)	X (CP94-Iam:CP94-25)	X (PP84-11:VP87-25)	N	0 (BGDR99-23:BP89-25)	<>	3 (BP89-32:BP89-25)
Supragenual (BA32)	3 (AP84-B:AP84-32)	X (BP89-46:BP89-32)	X (B88-Ig:B88-32)	N	Y (Insausti and Munoz (2001))	X (B88-23:B88-32)	3 (B89-25:B89-32)	<>

The anatomical connectivity as determined largely by queries to the Cocomac database (www.cocomac.org) and supplemented with searches to Pubmed (http://www.ncbi.nlm.nih.gov/entrez/query.fcgi?DB=pubmed) is shown. The matrix is read as column connecting to row, i.e. amygdala connects to BA 46 with reference "0 (PCG81-amg:W40-46)". Each cell is coded as follows: "0" represents no connection in all Cocomac references and therefore the path is not allowed in the model; "1", "2", or "3" represents the density of the label with "3" being the strongest; "X" represents the label being present but of unknown density; "Y" represents a confirmation of a connection based on a Pubmed search; "N" represents no reference found for the connection. A reference in parentheses follows each symbol. The references following "Y" are listed in the references section below. The references following all other symbols are described in (Kötter, 2004). All symbols except "0" represent paths that were allowed in the model.

minimize the impact of task-related coactivation on connectivity measures, which gave "residual activity" time series. This was done through a general linear model approach (as implemented in SPM99). Because our region selection is focused on areas showing significant task activation, our input data are therefore informed by the cognitive task, but not exclusively or largely driven by task-related activation changes. We have used this approach in previous analyses of effective connectivity to derive models in good agreement with known neuroanatomy and physiology (Meyer-Lindenberg et al., 2004; Pezawas et al., 2005). Extracted time series were then averaged across subjects for each region. These average time series are shown in Fig. 2. The pairwise correlations between the average time series for each region were used to compute the interregional correlation matrix, C, for the studied groups.

The effective degrees of freedom, υ, for each regional average time series were calculated from the data, using the autocorrelation structure of the average time series, assuming an AR(1) model (Kruggel et al., 2002) according to

$$\upsilon = (N-P)\left(\frac{1-\rho(1)^2}{1+\rho(1)^2}\right)$$

where N represents the number of time points in the MRI scan, P represents the number of regressors, and $\rho(1)^2$ is the squared first-order autocorrelation.

Following Bullmore et al. (2000), Principal Component Analysis (PCA) was used to estimate the residual variance, ψ_i, for each region i. The residual variance was estimated from the data as the ratio between the square of the first eigenvalue (λ_1^2) and the sum of the square of all m eigenvalues derived from the PCA of that region.

$$\psi_i = 1 - \frac{\lambda_1^2}{\sum_{j=1}^{m} \lambda_j^2}$$

Path analysis

The methodological goal of this study was to investigate an automated method of path model construction rather than using an *a priori* model as is the usual case in path analysis (Meyer-Lindenberg et al., 2005; Steele et al., 2004; Büchel and Friston, 1997). Starting from a nuclear model (Meyer-Lindenberg et al., 2005; Pezawas et al., 2005), new paths were added stepwise until an optimally explanatory, but parsimonious model was reached. The nuclear model was comprised of four predefined paths which were kept unconstrained from zero at every iteration resulting in an initial model with $q=4$ paths, where q is the number of paths unconstrained from zero. The connections of orbitofrontal cortex (OFC) to amygdala, amygdala to subgenual cingulate, subgenual cingulate to supragenual cingulate, and supragenual cingulate back to amygdala comprised our nuclear model. For all other regions, the model started with the $p(p-1)$ vector of path coefficients, θ, all constrained to zero for those paths.

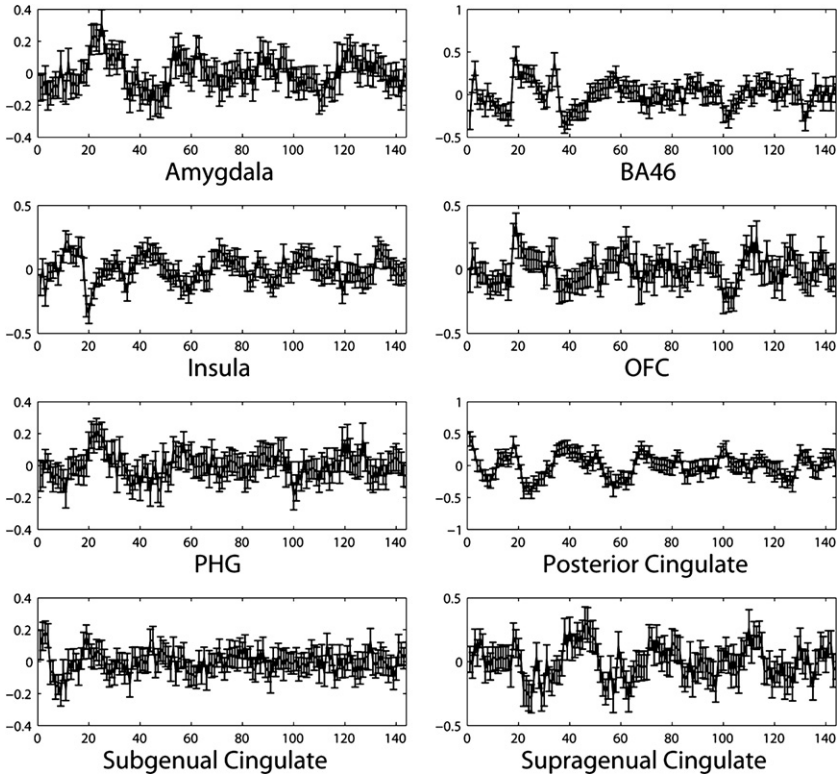

Fig. 2. Average time series from the first group of subjects for each of the eight regions used in the analysis. The time series from each of the eight regions labeled above was extracted from all the subjects in the first group of the data for each region and for each subject. Activation related to the task was subtracted from the time series. The time series were averaged across subjects and the mean across the 500 groups with standard deviation error bars is shown here. The horizontal axis gives the time in scans and the vertical axis gives the BOLD response in arbitrary units.

In the path analysis procedure, the correlation matrix predicted by the path model, $\Sigma(\theta)$, was derived using the Reticular Action Model (RAM) defined by the so-called McArdle–McDonald equation (McArdle and McDonald, 1984)

$$\Sigma(\theta) = (I - K)^{-1}\Psi((I - K)^{-1})'$$

where Ψ denotes a $(p \times p)$ diagonal matrix of the residual variances, ψ_i, for each region, K denotes the $(p \times p)$ path model matrix comprised of the vector of path coefficients, θ, and zeros along the diagonal, I denotes a $(p \times p)$ identity matrix, and $((I-K)^{-1})'$ denotes the transpose of the matrix operation.

The value of each unconstrained path coefficient in θ is found by iteratively minimizing the maximum likelihood discrepancy function

$$F(C,\Sigma(\theta)) = \log(\det(\Sigma(\theta))) + tr(C\Sigma^{-1}(\theta)) - \log(\det(C)) - p$$

in terms of the free components in θ. The value of $(\upsilon-1)\times F(C, \Sigma(\theta))$ is a chi-square approximation for the model with $1/2\ p\ (p+1)-q$ degrees of freedom.

In our analysis, this calculation was implemented in Matlab (Mathworks, Natick, MA) using Adaptive Simulated Annealing (ASA) (www.ingber.com) (Ingber, 1989) as an annealing minimization program that attends to some annealing schedule allowing the minimization search to explore a broad space. This is used to avoid finding values of θ that resulted in a local minimum. The ASA C code was interfaced to Matlab by use of the ASAMIN "mex" C code (www.econ.ubc.ca/ssakata/public_html). The minimization was started with random seed values for the coefficients, θ. Although we did not conduct a systematic study of differing minimization procedures, the annealing approach and previous successful application in a neuroimaging study (Steele et al., 2004) made ASA a reasonable choice for global minimization.

In order to specify or force a model onto a particular group, the matrix K can be specified *a priori*. However, in order to automatically derive the model, a gradient descent approach was used to find, at each step, the one path whose inclusion would most improve the model fit with the observed correlation matrix. The gradient descent approach was calculated for each possible path coefficient l in θ as a Modification Index, *MI*, according to a procedure in (Sorbom, 1989)

$$MI = \frac{1/2\hat{g}_l^2}{\hat{k}_l}$$

where $\hat{g}_l = \frac{\partial F}{\partial \theta_l}$ and $\hat{k}_l = \frac{\partial^2 F}{\partial \theta_l \partial \theta_l}$. The first order and second order partial derivatives can be approximated (Cudeck et al., 1993) according to

$$\frac{\partial F}{\partial \theta_l} = \frac{1}{2} tr\left(\Sigma^{-1}(\theta)[\Sigma(\theta) - C]\Sigma^{-1}(\theta)C_l\right)$$

$$\frac{\partial^2 F}{\partial \theta_l \partial \theta_l} = \frac{1}{2} tr\left(\Sigma^{-1}(\theta)C_l\Sigma^{-1}(\theta)C_l\right)$$

The matrix C_l comprises the partial derivatives of the modeled covariance with respect to the lth path coefficient and is defined as

$$C_l = \frac{\Sigma(\theta + e_l\eta) - \Sigma(\theta)}{\eta}$$

where e_l denotes a vector which has the length of the total possible number of path coefficients, $p(p-1)$, with all elements set to zero except at the lth position which is set to one, and η is an arbitrarily small constant set to $\eta = 10^{-4}$ for this experiment.

The value of MI approximates the estimate of how much better the model fits to the observed data when the coefficient l is unconstrained from zero. The path coefficient with the greatest MI value was therefore unconstrained from zero and incorporated into the model. To guide this iterative process, since addition of more paths always numerically improves the fit, it is necessary to use goodness of fit parameters dependent on model parsimony. Therefore we used Bollen's parsimonious fit index (Bollen, 1988), ρ, which adjusts for both the fit with the observed correlation matrix and the fewest number of paths possible. Bollen's parsimonious fit index ranges from zero to one with one being a perfectly parsimonious model, and is defined as

$$\rho = \frac{(\chi_0^2/k) - (\chi_q^2/k - q)}{\chi_0^2/k}$$

where χ_0^2 denotes the chi square for the model in which all path coefficients are set to zero, χ_q^2 denotes the chi square for the model with q nonzero paths, and k represents the number of non-redundant elements in the observed correlation matrix and the estimated residual variances $\left(k = \frac{1}{2}p(p+1)\right)$.

At each step, path coefficients resulting in the maximum increase of ρ relative to the previous step were incorporated into the model until no further improvement of parsimony was found. The process of automatic construction can be seen in Fig. 3.

The generated model was checked to prevent unidentified models which do not have unique solutions. In an unidentified model, the number of nonzero paths, q, is greater than the number of non-redundant elements in the observed correlation matrix and residual variances, k. Thus, in our model, q was always restricted to be less than k.

For validation, path models were automatically constructed for the first group of each of the 500 surrogate data sets. Then, the path model matrix automatically derived from the first group was forced on the independent data of the second group by specifying K. The model was considered validated for the pair when the model fit both the first and second group data of a pair with a threshold of $P > 0.05$. Furthermore, to assess the significance of individual paths, a mean and standard deviation were derived for each coefficient across all validated models from the first group. Those path coefficients in which the standard deviation from the mean did not cross zero were deemed to be significant and are discussed below.

For validation of the nuclear model, each path in the nuclear model was removed (forced to zero) one at a time from the first group automatically derived models. The modification index of that removed path was compared to the modification index of all other paths across the 500 groups in a repeated measures one-way ANOVA.

Results

A model was independently derived from the first of each group of 500 pairs. These models reached an average parsimonious fit index of $\rho = 0.75 \pm 0.07$, and all 500 derived models survived the $P > 0.05$ threshold. The maximum of the parsimonious fit index across all 500 groups is shown in Fig. 3.

For validation, the connections derived automatically from the first group in each pair were subsequently forced on the observed

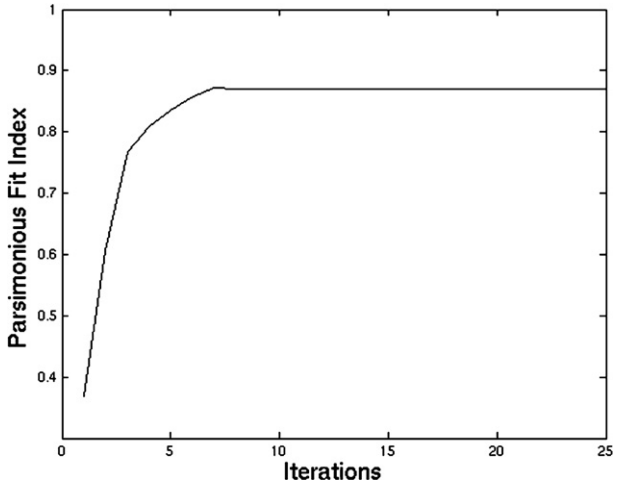

Fig. 3. Model fitting reached a maximum in parsimonious fit index. The automatically constructed model which reached the maximum in parsimony across the 500 groups is shown. During the automatic construction of each model, paths were iteratively unconstrained from zero. Each path increased the parsimonious fit index until a maximum was reached. The model was run over 25 iterations.

correlation matrix derived independently from the second group in that pair. 499 models which previously fit again survived the $P > 0.05$ threshold, meaning that the derived models could be independently validated inferentially in the second independent group of matched healthy subjects in all but one instance. The derived models were therefore both parsimonious and fit the observed data well.

In addition to validating the models as a whole in each pair, we also desired to see which individual path coefficients were consistent across pairs. For all the automatically derived models that fit both the data set on which they were derived (first group) and an independent matched data set (second group), the mean and standard deviation of the automatically derived path models were calculated for all paths and recorded for those path coefficients in which the standard deviation from the mean did not cross zero. Ten paths were found to make significant and consistent contributions across the groups. These significant paths and their corresponding coefficients are shown in Table 3 and Fig. 4.

The amygdala was found to be a hub of connections, having interactions with the parahippocampal gyrus (PHG), subgenual cingulate, OFC, posterior cingulate, insula, and supragenual cingulate. The paths from amygdala to PHG, supragenual cingulate to amygdala, and supragenual cingulate to posterior cingulate were especially strong.

In order to determine if the *a priori* nuclear model provided a good fit to the data, each path in the nuclear model was removed and the modification index of the removed path was compared to the distribution of modification indices for each coefficient. The results for this calculation are shown in Table 4. The modification index was significantly higher for the all the removed paths in the nuclear model than the distribution of modification indices for all the other paths. These high modification indices suggest that the nuclear model is justifiably included.

Discussion

In the present work, we used a data-driven approach to construct a parsimonious model of effective connectivity during neural processing of fearful stimuli that was validated using a bootstrapping approach in a large data set of healthy participants. Our data show that iterative search algorithms guided by known neuroanatomy are a feasible approach to the characterization of neural interactions in the human brain. The derived model confirms and extends previous results on human amygdala regulation.

Each of the path coefficients in the model represents a directional influence from one brain region to another across the time of the task. A positive (negative) coefficient is interpreted as the degree to which increases in BOLD activity in the parent region predict increases (decreases) in the child region. Since the signal is derived from the BOLD response, positive or negative coefficients cannot naively be assumed to represent excitation or inhibition, respectively. BOLD response is generally thought to be a combination of both excitatory and inhibitory input to a neuronal region that cannot be independently estimated using fMRI (Logothetis et al., 2001; Arthurs and Boniface, 2002) although some studies have shown neural excitatory input to be more representative of the BOLD signal (Waldvogel et al., 2000). Also, the neural understanding of a decrease in BOLD signal remains controversial (Harel et al., 2002; Raichle, 1998) but a recent study has shown that decreases in BOLD signal correlate to a suppression of neural activity (Shmuel et al., 2006).

Although establishing effective connectivity through path analysis is useful, it does have drawbacks. Path analysis uses covariances or correlations as the primary data, ignoring the arrow of time as well as any mutual information between regions which is not correlative (such as higher order or nonlinear dependencies). Dynamic Causal Modeling (DCM) is able to take this information into account and is also better able to represent neural interactions directly by explicitly modeling the dependence of BOLD signal on neural response (Penny et al., 2004). However, DCM also does require a predefined network of interaction and does not yet provide an inferential test of goodness of fit of the model. For both SEM and DCM, even if directionality is correctly estimated, modeling results do not prove causality but only infer how well the specified directional model is able to represent the given data. In SEM, the relevance of model fit, per se, for the neurobiological usefulness of a model of effective connectivity also depends on the specific question asked (Protzner and McIntosh, 2006). Additionally, our large data set enabled an extensive resampling procedure for model verification. If fewer subjects are available, other

Table 3
Significant path coefficients

Path	Mean value	Standard deviation
Amygdala → PHG	0.282	0.105
Amygdala → Subgenual	0.111	0.042
Insula → Amygdala	0.087	0.086
OFC → Amygdala	0.075	0.032
OFC → BA46	0.164	0.139
Posterior Cingulate → Amygdala	−0.074	0.049
Subgenual → Insula	0.066	0.051
Subgenual → Supragenual	0.054	0.045
Supragenual → Amygdala	−0.164	0.037
Supragenual → Posterior Cingulate	0.264	0.172

Path models automatically generated on the first group which also fit the independent second group were averaged. Those coefficients in which the standard deviation from the mean did not cross zero were deemed significant and are shown here.

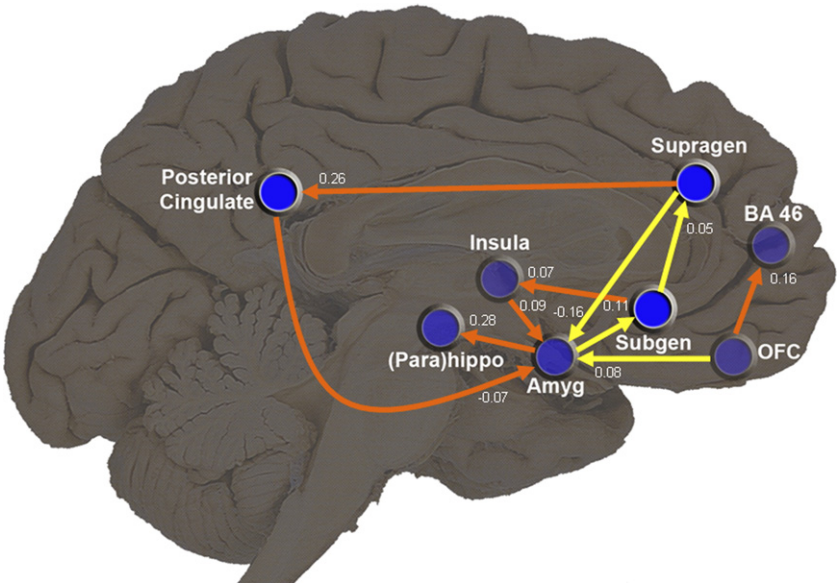

Fig. 4. Automatically derived path model. Yellow paths indicate those that were part of the nuclear model and forced to be in the model at every iteration. Orange paths were automatically derived from the data using the automated procedure. Each region is represented by circles, and coordinates of each region are given in Table 1. The transparency of the circles representing each region determines how far lateral (more transparent) or medial (less transparent) the regions are. Each number represents the path coefficient or the directional influences from one brain region to another across the time interval of the task. Each path shown here was significant according to the criteria defined above.

resampling methods, such as bootstrapping with replacement across pairs (non-independent pairs) could be used instead.

Here, we introduced an elaborative approach starting from a nuclear model based on previous work and iteratively adding additional paths. There is no guarantee that the model derived by this procedure is "the best" model possible, since an exhaustive search of the model space is not computationally feasible (Bullmore et al., 2000). However, features of the connectivity structure found in the present study are supported by an extensive body of previous work.

In particular, the loop linking amygdala to subgenual cingulate to supragenual cingulate and back to amygdala was backed by previous studies (Pezawas et al., 2005; Meyer-Lindenberg et al., 2005) and anatomical connectivity (Ghashghaei and Barbas, 2002; Paus, 2001; Phillips et al., 2003) and was supported by the current model. We have hypothesized that these results are consistent with a negative feedback loop for amygdala function in the context of fear extinction (Pezawas et al., 2005). The amygdala is hypothesized to feed bottom-up information to the subgenual cingulate regarding the emotional coloring of events (Amaral and Price, 1984; Phillips et al., 2003). The negative connection from supragenual cingulate back to amygdala is consistent with behavioral data in rodents where electrical stimulation of the medial prefrontal cortex (mPFC) causes inhibition of several nuclei within the amygdala decreasing fear response (Quirk et al., 2006; Maren and Quirk, 2004) as well as in humans where data suggest that the mPFC is an inhibitory input to the amygdala (Rauch et al., 2006). Interestingly, both the negative connection from supragenual cingulate to amygdala as well as a negative connection from posterior cingulate to amygdala made a significant contribution to the model. This indicates the importance of regulatory interactions of the amygdala activity with more posterior cingulate cortex. This interaction may have been missed by previous functional connectivity studies (Pezawas et al., 2005) that were focused on a part of the cingulate that also showed structural abnormalities in the context of a genetic effect. Of interest in this context is a subsequent study of another genetic variant implicated in amygdala dysregulation that did indeed show structural abnormalities in posterior cingulate (Meyer-Lindenberg et al., 2006).

Our model showed strong interactions of lateral prefrontal cortex (BA 46) with OFC. This is in good agreement with anatomical data in which OFC is extensively and reciprocally connected with dorsolateral prefrontal cortex (DLPFC) (Barbas and Pandya, 1989; Petrides and Pandya, 1999) as well as with previously derived models in which DLPFC exerts higher-level control over lower order regions in the context of emotion regulation (Meyer-Lindenberg et al., 2005;

Table 4
Nuclear model modification indices

	OFC → Amygdala	Supragenual → Amygdala	Amygdala → Subgenual	Subgenual → Supragenual
F-value	14.00	55.75	36.76	4.71
P-value	0.0045	<0.00001	<0.00001	0.034

To test the significance of each path in the nuclear model, each path within the nuclear model was separately forced to zero in the complete models derived across the first group in the 500 pairs. The modification index of that removed path was compared to the modification indices of all other paths in a repeated measures one-way ANOVA. The significance values for each modification index in the nuclear model versus the modification index of all other paths are shown.

Hariri et al., 2003; Levesque et al., 2003). The significant path derived in our model has directionality from BA46 to OFC, which may indicate the predominance of information flow from OFC into higher order areas.

Amydgala and the OFC are strongly anatomically interconnected (Ghashghaei and Barbas, 2002). OFC connections, especially with the amygdala, are critical for stimulus-reinforcement association learning (Pears et al., 2003) and are involved in changing learned behavior based on feedback, such as punishment (Kringelbach and Rolls, 2004). Together with this strong *a priori* evidence and our own previous SEM work (Meyer-Lindenberg et al., 2005), the present data further support the importance of this interaction in the connectivity structure of the limbic system by showing a consistent and independently significant contribution to the effective connectivity model derived here.

We observed a strong connection from amygdala to the PHG (including hippocampus), delineating a neural interaction thought to be essential to the processing of emotional memory (Saunders et al., 1988). Through increased interactions during observation of emotional stimuli, the amygdala–hippocampal connection has been observed to be enhanced during both memory encoding and consolidation in both animal models (McGaugh, 2000; McGaugh and Roozendaal, 2002) and human studies (Dolcos et al., 2004; Phelps, 2004; Smith et al., 2006). The connection in our model is thus consistent with experimental evidence for amygdala regulated hippocampal function in emotional memory.

In a larger context, Phillips et al. (2003) have hypothesized the existence of a dorsal and a ventral stream of emotional cognition, a proposal which is largely consistent with the interactions observed here. The ventral stream is posited to appraise emotional behavior and produce an affective state, whereas the dorsal stream acts as a regulatory mechanism for the ventral stream. The hypothesized ventral stream is comprised of the amygdala, subgenual cingulate, OFC, and insula. The insula and the amygdala have been implicated as part of both the identification of emotional significance of the stimulus and the production of an affective state in response to that stimulus (Calder et al., 2001). The OFC and subgenual cingulate have been shown through lesion and neuroimaging studies to affect the production of an emotional response to a stimulus (Paus, 2001; Kringelbach and Rolls, 2004). Our model quantifies interactions between these regions of the hypothesized ventral stream of emotional processing.

The dorsal system is comprised of supragenual cingulate, hippocampus, and lateral prefrontal cortex. All of these structures are important for emotional regulation, possibly through reciprocal interaction with structures in the ventral stream. The posterior cingulate is not explicitly named as being part of the dorsal stream; however, its location in the dorsal cingulate and strong negative connection to the amygdala observed here are consistent with a regulatory function with respect to the amygdala. Also the strong negative connection from supragenual cingulate to amygdala is consistent with the interpretation of a dorsal inhibitory stream regulating production of an affective response to an emotional stimulus by the ventral system.

In summary, we have derived and verified an effective connectivity network during processing of fearful and angry emotional stimuli in the human brain using fMRI. This model largely confirms and extends previous accounts of amygdala interactions in the context of emotional regulation (Pezawas et al., 2005; Phillips et al., 2003). We hope that this model will be usefully applied in the study of disease states hypothesized to affect connectivity in the brain, such as schizophrenia. It can also be used to study genetic variation impacting on connectivity and emotional processing, such as the COMT val157met variant (Drabant et al., 2006) and 5-HTTLPR, which has been shown to have an effect on functional connectivity (Pezawas et al., 2005). The application of an anatomically plausible and independently validated model should provide additional power in ascertaining subtle biological effects, complementing traditional neuroimaging analysis.

Acknowledgments

We would like to thank Dr. Douglas Steele for consultation on structural equation modeling. This research was supported by the Intramural Program of the National Institute of Mental Health.

References

Adolphs, R., Tranel, D., et al., 1994. Impaired recognition of emotion in facial expressions following bilateral damage to the human amygdala. Nature 372 (6507), 669–672.

Amaral, D.G., Price, J.L., 1984. Amygdalo-cortical projections in the monkey (*Macaca fascicularis*). J. Comp. Neurol. 230 (4), 465–496.

Arthurs, O.J., Boniface, S., 2002. How well do we understand the neural origins of the fMRI BOLD signal? Trends Neurosci. 25 (1), 27–31.

Barbas, H., De Olmos, J., 1990. Projections from the amygdala to basoventral and mediodorsal prefrontal regions in the rhesus monkey. J. Comp. Neurol. 300 (4), 549–571.

Barbas, H., Pandya, D.N., 1989. Architecture and intrinsic connections of the prefrontal cortex in the rhesus monkey. J. Comp. Neurol. 286 (3), 353–375.

Bertolino, A., Callicott, H.J., et al., 2001. The effect of treatment with antipsychotic drugs on brain *N*-acetylaspartate measures in patients with schizophrenia. Biol. Psychiatry 49 (1), 39–46.

Bollen, K.A., 1988. Structural Equations with Latent Variables. Wiley, New York.

Büchel, C., Friston, K.J., 1997. Modulation of connectivity in visual pathways by attention: cortical interactions evaluated with structural equation modelling and fMRI. Cereb. Cortex 7 (8), 768–778.

Bullmore, E., Horwitz, B., et al., 2000. How good is good enough in path analysis of fMRI data? NeuroImage 11 (4), 289–301.

Calder, A.J., Lawrence, D.A., et al., 2001. Neuropsychology of fear and loathing. Nat. Rev., Neurosci. 2 (5), 352–363.

Cavada, C., Company, T., et al., 2000. The anatomical connections of the macaque monkey orbitofrontal cortex. A review. Cereb. Cortex 10 (3), 220–242.

Cudeck, R., Klebe, J.K., et al., 1993. A simple Gauss-Newton procedure for covariance structure analysis with high-level computer languages. Psychometrika 58 (2), 211–232.

Dolcos, F., LaBar, K.S., et al., 2004. Interaction between the amygdala and the medial temporal lobe memory system predicts better memory for emotional events. Neuron 42 (5), 855–863.

Drabant, E.M., Hariri, R.A., et al., 2006. Catechol *O*-methyltransferase Val158Met genotype and neural mechanisms related to affective arousal and regulation. Arch. Gen. Psychiatry 63 (12), 1396–1406.

Ekman, P., Friesen, W.V., 1976. Pictures of Facial Affect. Consulting Psychologists Press, Palo Alto.

Ghashghaei, H.T., Barbas, H., 2002. Pathways for emotion: interactions of prefrontal and anterior temporal pathways in the amygdala of the rhesus monkey. Neuroscience 115 (4), 1261–1279.

Harel, N., Lee, P.S., et al., 2002. Origin of negative blood oxygenation level-dependent fMRI signals. J. Cereb. Blood Flow Metab. 22 (8), 908–917.

Hariri, A.R., Bookheimer, Y.S., et al., 2000. Modulating emotional responses: effects of a neocortical network on the limbic system. NeuroReport 11 (1), 43–48.

Hariri, A.R., Mattay, S.V., et al., 2002. Serotonin transporter genetic variation and the response of the human amygdala. Science 297 (5580), 400–403.

Hariri, A.R., Mattay, S.V., et al., 2003. Neocortical modulation of the amygdala response to fearful stimuli. Biol. Psychiatry 53 (6), 494–501.

Ingber, L., 1989. Very fast simulated re-annealing. Math. Comput. Model. 12 (8), 967–973.

Insausti, R., Munoz, M., 2001. Cortical projections of the non-entorhinal hippocampal formation in the cynomolgus monkey (*Macaca fascicularis*). Eur. J. Neurosci. 14 (3), 435–451.

Kobayashi, Y., Amaral, D.G., 2003. Macaque monkey retrosplenial cortex: II. Cortical afferents. J. Comp. Neurol. 466 (1), 48–79.

Kötter, R., 2004. Online retrieval, processing, and visualization of primate connectivity data from the CoCoMac database. Neuroinformatics 2 (2), 127–144.

Kringelbach, M.L., Rolls, E.T., et al., 2004. The functional neuroanatomy of the human orbitofrontal cortex: evidence from neuroimaging and neuropsychology. Prog. Neurobiol. 72 (5), 341–372.

Kruggel, F., Pelegrini-Issac, M., et al., 2002. Estimating the effective degrees of freedom in univariate multiple regression analysis. Med. Image Anal. 6 (1), 63–75.

LeDoux, J.E., 2000. Emotion circuits in the brain. Annu. Rev. Neurosci. 23, 155–184.

Levesque, J., Eugene, F., et al., 2003. Neural circuitry underlying voluntary suppression of sadness. Biol. Psychiatry 53 (6), 502–510.

Logothetis, N.K., Pauls, J., et al., 2001. Neurophysiological investigation of the basis of the fMRI signal. Nature 412 (6843), 150–157.

Maren, S., Quirk, G.J., 2004. Neuronal signalling of fear memory. Nat. Rev., Neurosci. 5 (11), 844–852.

Mayberg, H.S., Liotti, M., et al., 1999. Reciprocal limbic-cortical function and negative mood: converging PET findings in depression and normal sadness. Am. J. Psychiatry 156 (5), 675–682.

McArdle, J.J., McDonald, R.P., 1984. Some algebraic properties of the Reticular Action Model for moment structures. Br. J. Math Stat. Psychol. 37 (Pt. 2), 234–251.

McGaugh, J.L., 2000. Memory—A century of consolidation. Science 287 (5451), 248–251.

McGaugh, J.L., Roozendaal, B., 2002. Role of adrenal stress hormones in forming lasting memories in the brain. Curr. Opin. Neurobiol. 12 (2), 205–210.

McIntosh, A.R., Gonzalez-Lima, F., 1994. Structural Equation Modeling and its application to network analysis in functional brain imaging. Human Brain Mapping 2, 2–22.

Meyer-Lindenberg, A., Kohn, P., et al., 2004. Neural basis of genetically determined visuospatial construction deficit in Williams syndrome. Neuron 43 (5), 623–631.

Meyer-Lindenberg, A., Hariri, R.A., et al., 2005. Neural correlates of genetically abnormal social cognition in Williams syndrome. Nat. Neurosci. 8 (8), 991–993.

Meyer-Lindenberg, A., Buckholtz, W.J., et al., 2006. Neural mechanisms of genetic risk for impulsivity and violence in humans. Proc. Natl. Acad. Sci. U. S. A. 103 (16), 6269–6274.

Morecraft, R.J., Geula, C., et al., 1992. Cytoarchitecture and neural afferents of orbitofrontal cortex in the brain of the monkey. J. Comp. Neurol. 323 (3), 341–358.

Morris, J.S., Frith, D.C., et al., 1996. A differential neural response in the human amygdala to fearful and happy facial expressions. Nature 383 (6603), 812–815.

Mufson, E.J., Mesulam, M.M., 1982. Insula of the old world monkey: II. Afferent cortical input and comments on the claustrum. J. Comp. Neurol. 212 (1), 23–37.

Papez, J.W., 1995. A proposed mechanism of emotion. 1937. J. Neuropsychiatry Clin. Neurosci. 7 (1), 103–112.

Paus, T., 2001. Primate anterior cingulate cortex: where motor control, drive and cognition interface. Nat. Rev., Neurosci. 2 (6), 417–424.

Pears, A., Parkinson, A.J., et al., 2003. Lesions of the orbitofrontal but not medial prefrontal cortex disrupt conditioned reinforcement in primates. J. Neurosci. 23 (35), 11189–11201.

Penny, W.D., Stephan, E.K., et al., 2004. Modeling functional integration: a comparison of structural equation and dynamic causal models. NeuroImage 23 (Suppl. 1), S264–S274.

Petrides, M., Pandya, D.N., 1999. Dorsolateral prefrontal cortex: comparative cytoarchitectonic analysis in the human and the macaque brain and corticocortical connection patterns. Eur. J. Neurosci. 11 (3), 1011–1036.

Pezawas, L., Meyer-Lindenberg, A., et al., 2005. 5-HTTLPR polymorphism impacts human cingulate-amygdala interactions: a genetic susceptibility mechanism for depression. Nat. Neurosci. 8 (6), 828–834.

Phelps, E.A., 2004. Human emotion and memory: interactions of the amygdala and hippocampal complex. Curr. Opin. Neurobiol. 14 (2), 198–202.

Phillips, M.L., Drevets, C.W., et al., 2003. Neurobiology of emotion perception I: the neural basis of normal emotion perception. Biol. Psychiatry 54 (5), 504–514.

Protzner, A.B., McIntosh, A.R., 2006. Testing effective connectivity changes with structural equation modeling: what does a bad model tell us? Hum. Brain Mapp. 27 (12), 935–947.

Quirk, G.J., Garcia, R., et al., 2006. Prefrontal mechanisms in extinction of conditioned fear. Biol. Psychiatry 60 (4), 337–343.

Raichle, M.E., 1998. Behind the scenes of functional brain imaging: a historical and physiological perspective. Proc. Natl. Acad. Sci. U. S. A. 95 (3), 765–772.

Rauch, S.L., Shin, M.L., et al., 2006. Neurocircuitry models of posttraumatic stress disorder and extinction: human neuroimaging research-past, present, and future. Biol. Psychiatry 60 (4), 376–382.

Saunders, R.C., Rosene, L.D., et al., 1988. Comparison of the efferents of the amygdala and the hippocampal formation in the rhesus monkey: II. Reciprocal and non-reciprocal connections. J. Comp. Neurol. 271 (2), 185–207.

Shmuel, A., Augath, M., et al., 2006. Negative functional MRI response correlates with decreases in neuronal activity in monkey visual area V1. Nat. Neurosci. 9 (4), 569–577.

Smith, A.P., Stephan, E.K., et al., 2006. Task and content modulate amygdala–hippocampal connectivity in emotional retrieval. Neuron 49 (4), 631–638.

Sorbom, D., 1989. Model modification. Psychometrika 54 (3), 371–384.

Steele, J.D., Meyer, M., et al., 2004. Neural predictive error signal correlates with depressive illness severity in a game paradigm. NeuroImage 23 (1), 269–280.

Stefanacci, L., Suzuki, A.W., et al., 1996. Organization of connections between the amygdaloid complex and the perirhinal and parahippocampal cortices in macaque monkeys. J. Comp. Neurol. 375 (4), 552–582.

Waldvogel, D., van Gelderen, P., et al., 2000. The relative metabolic demand of inhibition and excitation. Nature 406 (6799), 995–998.